Electronic Supplementary Material (ESI) for Journal of Materials Chemistry C.

Supplementary Information

3D printing of tunable shape memory polymer blends

Siyuan Chen, Qinglong Zhang, and Jiachun Feng*

***Corresponding author's email: jcfeng@fudan.edu.cn**

1. Experimental Section

Blending and Extrusion Process: 30 wt% SEBS (G1654, Kraton, Texas), 50 wt% PEW (Qingdao Bouni Chem. Co. Ltd, China) and 20 wt% LDPE (N150, Sinopec Shanghai Petrochem. Co., China) were blended and extruded as monofilaments using a two screw extruder (HAAKE Polylab OS, ThermoFisher, Massachusetts). The speed of main screws was 35 rpm. Pressure on main screws was 10 bar. Temperature of zone 1-6 was 180, 200, 210, 220, 170 and 140 ^{o}C, respectively. The monofilament's diameter was 1.65±0.10 mm.

Quantitative Shape Memory Testing: The filament was cut up and molded as sheets at 200 ^{o}C for 5 min. Sheet with a length of 30 mm was immersed into a water bath with a temperature T_{d1} for 5 min, and bended by an angel of $\theta_{1,load}$. Then the sheet was cooled to T_{d2} while holding the stress for another 5 min. Internal stress of the sheet was quickly released, meaning the fixing of this first bending state. The fixed bending angel θ_1 was recorded. Afterwards, the sheet was further bended to an angel of $\theta_{2,load}$ and cooled to T_{d3} for shape fixing while holding the stress for 5 min. The fixed bending angel θ_2 was recorded when internal stress was released. Subsequently, the sheet was bended to an angel of $\theta_{3,load}$ and cooled to 0 ^{o}C. Similarly, the fixed bending angel θ_3 was recorded. After programming, the sheet was immersed into water bath of T_{d3}, T_{d2}, T_{d1} in sequence to achieve unconstrained shape recovery. Then the resultant bending angel was obtained as $\theta_{2,rec}$, $\theta_{1,rec}$, $\theta_{0,rec}$. R_f and R_r was calculated according to equation 1 and 2 as follows:

$$R_f(A\rightarrow B)=(\theta_B-\theta_A)/(\theta_{B,load}-\theta_A) \quad (1)$$

$$R_r(B\rightarrow A)=(\theta_B-\theta_{A,rec})/(\theta_B-\theta_A) \quad (2)$$

A and B represent shape 0, 1, 2 or 3.

Multi-stage Recovery Testing: The flat sheet was immersed into a water bath of 95 ^{o}C and deformed to a bending angel of approximately 180^{o}. After cooling to 0 ^{o}C and fixing the temporary shape, the sheet was reheated from 0 to 95 ^{o}C slowly. R_r was recorded at an interval of 5 ^{o}C. The whole testing took about 45 min.

Temperature Memory Effect Testing: Samples were bended to an angle of 90^{o} at different temperatures. After cooled to 0 ^{o}C and the temporary shapes fixed, samples were reheated to the bending temperatures and the recovery ratio was recorded. Keep heating until the maximum R_r of the sample was observed.

Thermal Characterization: SEBS, PEW, LDPE and ternary blends were evaluated by DSC on a Mettler DSC-821e apparatus (Mettler Toledo, Switzerland). The temperature range was from 0 to 200 ^{o}C. The heating and cooling rate was 10 ^{o}C min^{-1}. Additionally, successive nucleation and annealing thermal fractionation (SNA) was carried out follows: first of all, samples were heated to 200 ^{o}C to eliminate thermal history and cooled to 0 ^{o}C to create a standard thermal history. Secondly, samples were heated to the first seeding temperature (T_s) at 10 ^{o}C min^{-1} and held for 10 min. Thirdly, samples were cooled to 0 ^{o}C at 10 ^{o}C min^{-1}. The temperature range of thermal fractionation was from 105 to 30 ^{o}C at an interval of 5 ^{o}C. Finally, samples were reheated from 0 to 200 ^{o}C at 2 ^{o}C min^{-1}.

3D Printing Process: Monofilament made of the ternary blends was used to 3D print different structures by a FDM 3D printer (Maxform, Shenzhen Clopx. Co. Ltd, China). Temperature of nozzle and platform was 220 and 100 ^{o}C, respectively.

Morphology characterization: Crystalline morphologies of the SMPs were observed using DM2500P polarized optical microscope (POM) (Leica, Germany) with Linkam-THMS600 hot stage and Multimode 8 atom force microscope (AFM) (Bruker, German) with PeakForce quantitative nanomechanical property mapping (QNM) mode. Under PeakForce QNM mode, the formation of images is based on difference of modulus or adhesion. A transmission electron microscopy (TEM) (FEI, American) was used to investigate the morphology of the samples after stained by 4% RuO_4 (aq) for 3 hours.

2. Additional Experimental Results and Discussions

2.1 Effect of Mixing Ratio on Shape Memory Properties of the Ternary Blends

We prepared a series of samples with different mixing ratio (**Table S1**) and investigated the dual, triple and quadruple shape memory properties of these samples to elucidate the effect of the mixing ratio on the shape memory properties of the ternary blends. Corresponding bending angle (**Table S2, S3 and S4**) during the shape memory cycle was recorded and R_f/R_r values (**Table S5, S6 and S7**) were calculated according to equation 1 and 2 in the experimental section.

Table S1. Designations and composition of the ternary blends

Designation	Content (mass portion)		
	SEBS	**PEW**	**LDPE**
①	10	70	20
②	30	50	20
③	50	30	20
④	70	10	20
⑤	30	50	10
⑥	30	50	30

Table S2. Bending angle of samples during dual shape memory testing (T_{d1} = 80 ^oC)

Designation	**80 ^oC**	**0 ^oC**	**80 ^oC**
	θ_0 (^{o})	**$\theta_{1,load}/\theta_1$ (^{o})**	**$\theta_{0,rec}$ (^{o})**
①	0	90/90	10
②	0	90/87	3
③	0	90/85	2
④	0	90/70	0
⑤	0	90/87	2
⑥	0	90/86	11

Table S3. Bending angle of samples during triple shape memory testing (T_{d1} = 90 ^oC, T_{d2} = 60 ^oC)

Designation	**90 ^oC**	**60 ^oC**	**0 ^oC**	**60 ^oC**	**90 ^oC**
	θ_0 (^{o})	**$\theta_{1,load}/\theta_1$ (^{o})**	**$\theta_{2,load}/\theta_2$ (^{o})**	**$\theta_{1,rec}$ (^{o})**	**$\theta_{0,rec}$ (^{o})**
①	0	45/45	90/89	52	8
②	0	45/44	90/87	50	4
③	0	45/43	90/82	48	2
④	0	45/32	90/74	36	0
⑤	0	45/44	90/88	49	3
⑥	0	45/42	90/86	53	12

Table S4. Bending angle of samples during quadruple shape memory testing (T_{d1} = 95 ^oC, T_{d2} = 80 ^oC, T_{d3} = 65 ^oC)

Designation	95 ^oC	80 ^oC	65 ^oC	0 ^oC	65 ^oC	80 ^oC	95 ^oC
	θ_0 (^{o})	$\theta_{1,load}/\theta_1$(^{o})	$\theta_{2,load}/\theta_2$(^{o})	$\theta_{3,load}/\theta_3$(^{o})	$\theta_{2,rec}$ (^{o})	$\theta_{1,rec}$ (^{o})	$\theta_{0,rec}$ (^{o})
①	0	45/40	90/83	135/133	99	58	17
②	0	45/35	90/80	135/132	88	45	10
③	0	45/33	90/78	135/128	85	40	6
④	0	45/26	90/64	135/118	70	31	3
⑤	0	45/36	90/82	135/133	89	45	7
⑥	0	45/34	90/79	135/132	95	51	16

Table S5. R_f/R_r values of samples during dual shape memory testing (T_{d1} = 80 ^oC)

Designation	R_f(S0→S1) [%]	R_r(S1→S0$_{rec}$) [%]
①	100	89
②	97	97
③	94	98
④	78	100
⑤	97	98
⑥	96	87

Table S6. R_f/R_r values of samples during triple shape memory testing (T_{d1} = 90 ^oC, T_{d2} = 60 ^oC)

Designation	R_f(S0→S1) [%]	R_f(S1→S2) [%]	R_r(S2→S1$_{rec}$) [%]	R_r(S1$_{rec}$→S0$_{rec}$) [%]
①	100	98	84	85
②	98	93	86	92
③	96	83	87	96
④	71	72	90	100
⑤	98	96	89	94
⑥	93	92	75	77

Table S7. R_f/R_r values of samples during quadruple shape memory testing (T_{d1} = 95 ^oC, T_{d2} = 80 ^oC, T_{d3} = 65 ^oC)

Designation	R_f(S0→S1) [%]	R_f(S1→S2) [%]	R_f(S2→S3) [%]	R_r(S3→S2$_{rec}$) [%]	R_r(S2$_{rec}$→S1$_{rec}$) [%]	R_r(S1$_{rec}$→S0$_{rec}$) [%]
①	89	86	96	68	69	71
②	78	82	95	85	81	78
③	73	79	88	86	87	85
④	58	59	76	88	89	90
⑤	80	85	96	86	83	84
⑥	76	80	95	70	72	69

By analyzing the R_f/R_r values of 10SEBS/70PEW/20LDPE, 30SEBS/50PEW/20LDPE, 50SEBS/30PEW/20LDPE and 70SEBS/10PEW/20LDPE (①②③④), we come to the conclusion that: (i) The higher the content of SBES is, the higher the R_r value will be; (ii) The higher the content of PEW is, the higher the R_f value will be.

By analyzing the R_f/R_r values of 30SEBS/50PEW/10LDPE, 30SEBS/50PEW/20LDPE and 30SEBS/50PEW/30LDPE (②⑤⑥), we come to the conclusion that: (i) The higher the content of LDPE is, the lower the R_f and R_r value will be.

In brief, increasing the mass ratio of SEBS is beneficial to strengthen the capability of the sample to be restored to its previous shapes. In the contrast, increasing the mass ratio of PEW is beneficial to enhance the capability of the sample to fix temporary shapes. While LDPE has a negative influence both on fixing and recovery ability, especially for recovery ability. After comprehensive consideration, we hold the view that the ternary blends consisting of 30SEBS, 50 PEW and 20 LDPE has satisfactory fixing capability and recovery capability as well as good processability.

2.2 Discussion on the Relationship between R_f (R_r) Values and Enthalpy Values

As shown in **Fig. S1(a)**, to simulate the dual shape memory programming with DSC, we performed following treatment: the sample of the ternary blends was initially kept at 190 ^oC for 5 min and then it was cooled to 0 ^oC at 10 ^oC min^{-1} to create a standard thermal history. Subsequently, the sample was reheated to T_d at 30 ^oC min^{-1} and kept for 5 min. Then it was cooled to 0 ^oC at 30 ^oC min^{-1} and kept for 5 min. After complete crystallization, the sample was heated to T_d at 30 ^oC min^{-1} again and kept for 5 min to ensure steady state. At last, the sample was heated to 190 ^oC at 10 ^oC min^{-1}. The enthalpy in **Fig. S1(b)** and corresponding R_f (R_r) values were summed up roughly in **Table S8**. We found that the R_f and R_r values increase gradually when we choose larger T_d. What's more, there is a positive correlation between R_f (R_r) values and the enthalpy values. The simulated DSC procedure of quadruple shape memory behavior in **Fig. S1(c)** was similar with that in Fig. S1(a). In **Fig. S1(d)**, three exothermic peaks can be distinguished clearly in the range of fixing, which locate between 95 and 80 ^oC, between 80 and 65 ^oC and below 65 ^oC. Likewise, there are three endothermic peaks in the range of recovery. We notice that all the thermal transitions are totally separated and independent, which ensures that the excellent multiple shape memory behavior is valid. It should also be noticed that most of enthalpy change is located in non-isothermal sections and little heat variation can be observed in isothermal sections, which indicates that the thermal transition of this ternary blends is very rapid.

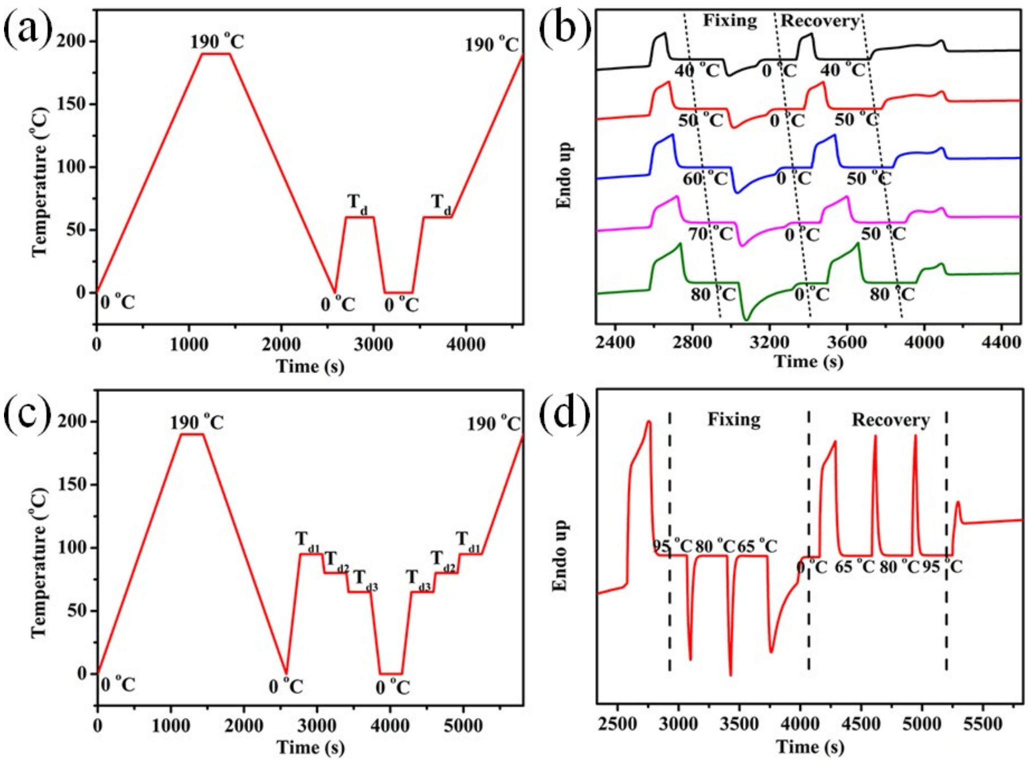

Fig. S1. The DSC procedures and results of thermal simulation testing. (a) DSC procedure simulating dual shape memory behavior with different T_ds. (b) Thermal result of simulated dual shape memory testing. (c) DSC procedure simulating quadruple shape memory behavior with T_{d1} of 95 °C, T_{d2} of 80 °C and T_{d3} of 65 °C. (d) Thermal result of simulated quadruple shape memory testing.

Table S8. R_f, R_r values of dual shape memory testing and corresponding enthalpy

	R_f (%)	R_r (%)	Enthalpy of fixing (J/g)	Enthalpy of recovery (J/g)
Td=40 °C	64	64	-28.8	27.9
Td=50 °C	80	83	-40.5	38.6
Td=60 °C	91	89	-73.3	70.0
Td=70 °C	96	93	-96.8	99.5
Td=80 °C	97	97	-124.1	119.8

2.3 Temperature Memory Effect of the Ternary Blends (30SEBS/50PEW/20LDPE)

This ternary blend can remember not only temporary shapes, but also the deformation temperatures. As shown in **Table S9**, the samples were deformed at different temperatures within the broad range of thermal transition and then cooled to 0 °C to fix the temporary shapes. When reheated to foregoing deformation temperatures, samples exhibit good recovery ratio. While the best recovery phenomenon always occurs at the temperature slightly higher than the corresponding deformation temperature until the crystalline components melt more completely.

Table S9. Temperature memory effect of the ternary blend (30SEBS/50PEW/20LDPE)

Deformation temperature (°C)	Recovery ratio at the deformation temperature (%)	Temperature with the best recovery (°C)
50	83	57
55	85	59
60	89	63
65	92	68
70	93	72
75	95	77
80	97	81
85	99	85
90	100	90
95	100	95

2.4 Shape Memory Testing Based on Continuous Heating Mode

Firstly, specimens were programmed as follows to generate different number of temporary shapes: Sample was deformed at 80 °C (T_{d1} = 80 °C) and cooled at 0 °C to generate one temporary shape. Similarly, to obtain specimen with two temporary shapes, two T_ds (T_{d1} = 90 °C, T_{d2} = 60 °C) were selected to bend the same part of the sample and the final cooling temperature is 0 °C. For specimen with three temporary shapes, we bended the same part of the sample at three different temperatures (T_{d1} = 95 °C, T_{d2} = 80 °C, T_{d3} = 65 °C) in sequence and the final cooling temperature is 0 °C, too. After programming, the specimens were immersed into water bath of 0 °C. Then we impose continuous heating on the specimens and monitored the bending angle in real time during triggering process. To exhibit the recovery process more conveniently under continuous heating, we adopted the following equation to calculate the overall recovery ratio ($R_{r,overall}$):

$$R_{r,overall} = \frac{\theta_{prog} - \theta(T)}{\theta_{prog}} \times 100\% \qquad (3)$$

Here, θ_{prog} is defined as the bending angle of fully programmed sample, θ(T) is the bending angle of the sample at corresponding temperature during recovery process. Temperature versus time plots were also recorded to calculate the heating rate. As shown in **Fig. S2**, the temperature of water bath increased approximately linearly with testing time during the experiment. We experimented with two constant heating rate (about 1 $K \cdot min^{-1}$ and 5 $K \cdot min^{-1}$).

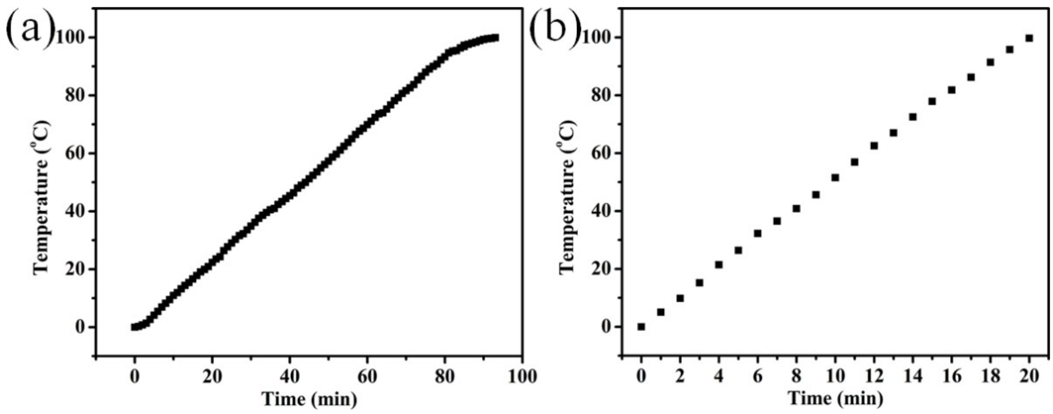

Fig. S2. Temperature of water bath versus testing time diagram. (a) Heating rate was about 1 $K \cdot min^{-1}$. (b) Heating rate was about 5 $K \cdot min^{-1}$.

When the heating rate was 1 K·min-1, the bending angle of sample versus temperature was monitored and $R_{r,overall}$ was and calculated, as shown in **Fig. S3**. With regards to sample with only one temporary shape, the bending angle grew smaller gradually with temperature increasing (See **Fig. S3(a)**). However, the bending angle did not decrease to 0 ^{o} when temperature rose to T_{d1} of 80 ^{o}C. Only when temperature rose to 90 ^{o}C, the bending angle became 0^{o}, resulting in full recovery (See in **Fig. S3(d)**). Similarly, for sample with two temporary shapes, the bending angle also decreased when heated (See in **Fig. S3(b)**), indicating a continuous recovery process (See in **Fig. S3(e)**). We notice that when heated to T_{d2} of 60 ^{o}C and T_{d1} of 90 ^{o}C, the recovery process slowed down but still continued. However, only when temperature rose to 72 ^{o}C, the sample recovered to S1. When temperature rose to 94 ^{o}C, the sample recovered to S0 completely. For sample with three temporary shapes, similar phenomenon was observed (See in **Fig. S3(c)** and **S3(f)**): temperature corresponding to complete recovery to S2, S1 and S0 was 71, 87 and 98 ^{o}C, respectively, higher than T_{d3} of 65 ^{o}C, T_{d2} of 80 ^{o}C, T_{d1} of 95 ^{o}C. According to above experiments, we may conclude that: (i) The bending angle grows smaller when heated with a constant rate, indicating a continuous recovery process. (ii) When heated around the priorly used T_ds, the recovery process slows down but still continues. (iii) A temperature slightly higher than corresponding T_d can result in a full recovery phenomenon.

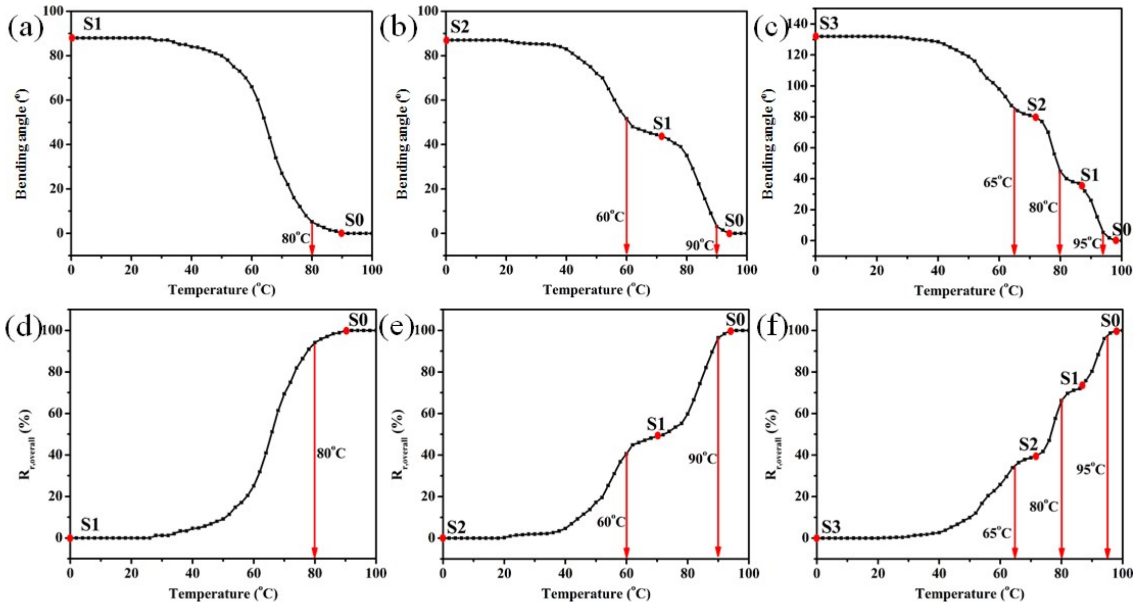

Fig. S3. Bending angle of sample with (a) one, (b) two and (c) three temporary shapes versus temperature diagram when the constant heating rate was about 1 K·min^{-1}. $R_{r,overall}$ of sample with (d) one, (e) two and (f) three temporary shapes versus temperature diagram when the constant heating rate was about 1 K·min^{-1}.

To further prove above-mentioned conclusions we used another constant heating rate (5 K·min^{-1}) to test again, as described in **Fig. S4**. Almost the same phenomenon was observed. To investigate the relationship between recover ratios and heating rate, a comparative analysis was performed between **Fig. S3** and **Fig. S4** (S3(d) versus S4(d), S3(e) versus S4(e), S3(f) versus S4(f)). It demonstrates that a higher heating rate leads to a slightly higher temperature for full recovery to each temporary shape, and changing heating rate did not result in the occurrence of new intermediate shapes. We think that there is a slight response delay when our material is exposed to a much higher heating rate, accounting for above-mentioned phenomenon. Actually, our material has a relatively good thermal sensitivity, hence the influence of different heating rate on recovery ratios is not very great.

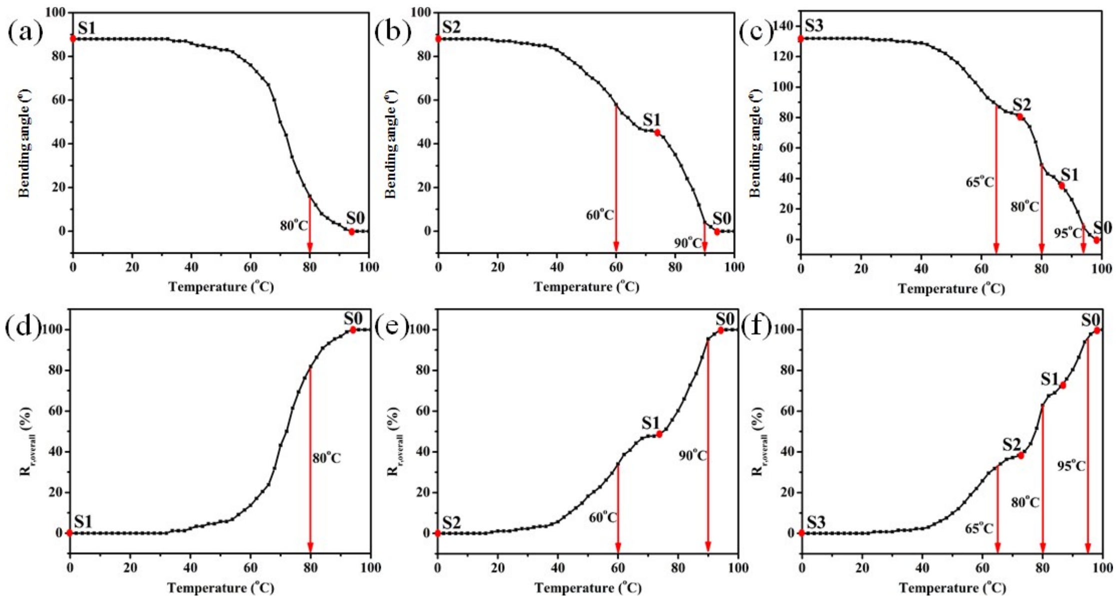

Fig. S4. Bending angle of sample with (a) one, (b) two and (c) three temporary shapes versus temperature diagram when the constant heating rate was about 5 K·min^{-1}. $R_{r,overall}$ of sample with (d) one, (e) two and (f) three temporary shapes versus temperature diagram when the constant heating rate was about 5 K·min^{-1}.

2.5 Morphology of Different Samples

The morphology of samples with different component was presented by transmission electron microscopy (TEM), polarized optical microscope (POM), and atomic force microscopy (AFM).

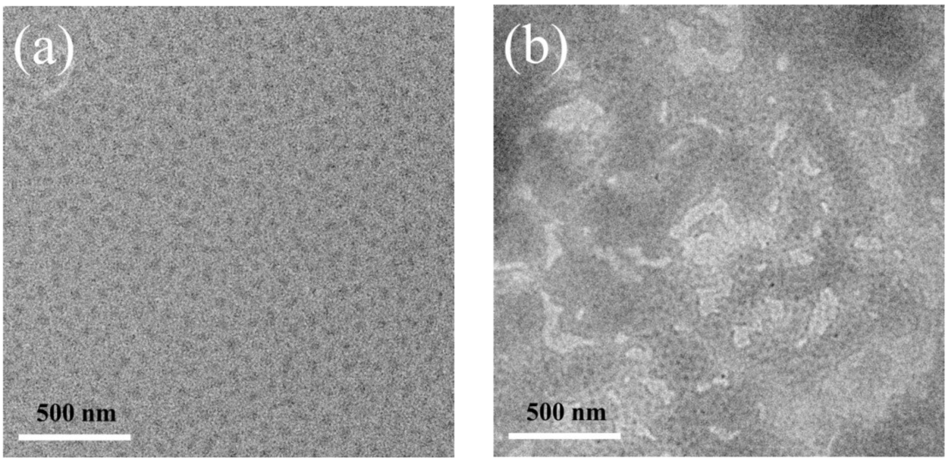

Fig. S5. TEM micrographs of (a) 100SEBS and (c) 30SEBS/50PEW/20LDPE.

TEM images of neat SEBS and 30SEBS/50PEW/20LDPE are shown in **Fig S5**. Both of the samples were stained by 4% RuO_4 (aq) for 3 hours in advance to distinguish various types of substance. Dark characteristics correspond to S-rich microdomains which are preferentially stained with electron-dense RuO_4. In **Fig. S5(a)**, the pure SEBS exhibits typical sea-island two-phase separation morphology. S-rich spherical microdomains with a diameter about 40 nm are randomly scattered in homogenous EB-rich matrix. With regards to the ternary blend (30SEBS/50PEW/20LDPE, see **Fig. S5(b)**), continuous SEBS phase still exists, indicating a complete and uniform SEBS-network. However, relatively larger-scaled phase separation occurs due to the addition of PEW and LDPE. The possible interpretation of this phenomenon is presented as follows: Both PEW and LDPE molecules are midblock-selectively compatible with SEBS, which means they will preferentially enter and swell in EB phase. Therefore, a percolation of PEW and LDPE molecules will form in the composite. However, when excessive amount of PEW and LDPE is added into SEBS, EB phase cannot take in all the PEW/LDPE molecules. Consequently, some of the "free" PEW/LDPE molecules aggregate outside the EB-rich phase, resulting in the formation of large-scaled SEBS-rich phase and PEW/LDPE-rich phase. It is worth emphasizing that although relatively large-scaled PE-rich phase present, the ternary blend still have good tunable shape memory effect and satisfactory processability.

PEW and LDPE are semicrystalline materials and exhibit strong birefringence under polarized light while SEBS possesses negligible crystallinity. Hence the dispersion of PEW and LDPE in SEBS matrix can be observed easily via POM. Samples were firstly heated to 200 ^{o}C and held for 5 min. Then the crystalline process of LDPE and PEW was observed at a cooling rate of 2 $K \cdot min^{-1}$. As shown in **Fig. S6(a)**, neat SEBS does not crystallize during cooling. As shown in **Fig. S6 (b)**, sample consisting of 10SEBS/70PEW/20LDPE starts to crystallize at approximately 85 °C. When mass portion of SEBS increases to 30 and 70, samples start to crystallize at 82 and 78 ^{o}C, respectively, indicating that SEBS has restriction on crystallization behavior of PEW and LDPE (See in **Fig. S6 (c)** and **S6 (d)**). For 30SEBS/50PEW/20LDPE, we notice that the distribution of crystallization is uniform on a POM's scale (**Fig. S6 (c)**), which demonstrates that PEW and LDPE molecules disperse uniformly in SEBS matrix when this mass ratio is taken. In the contrast, sample consisting of 10SEBS/70PEW/20LDPE always has two-phase morphology during the whole cooling process (**Fig. S6 (b)**). This can be explained that a small amount of SEBS cannot wrap all the PEW and LDPE, resulting in a large-scaled phase separation. When the mass portion of SEBS/PEW/LDPE is 70/10/20, too much SEBS severely hiders the crystallization process of PEW and LDPE, leading to a special crystallization morphology (**Fig. S6 (d)**).

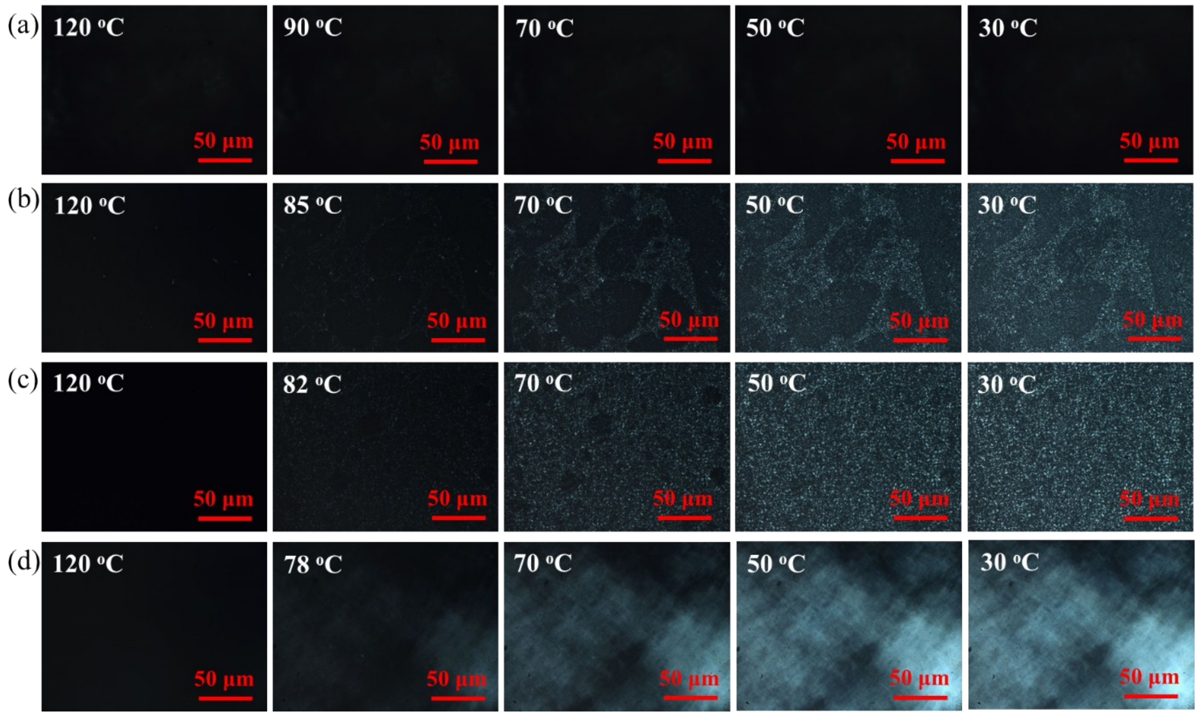

Fig. S6. POM images of (a) 100SEBS, (b) 10SEBS/70PEW/20LDPE, (c) 30SEBS/50PEW/20LDPE and (d) 70SEBS/10PEW/20LDPE when cooling at 2 K·min^{-1}.

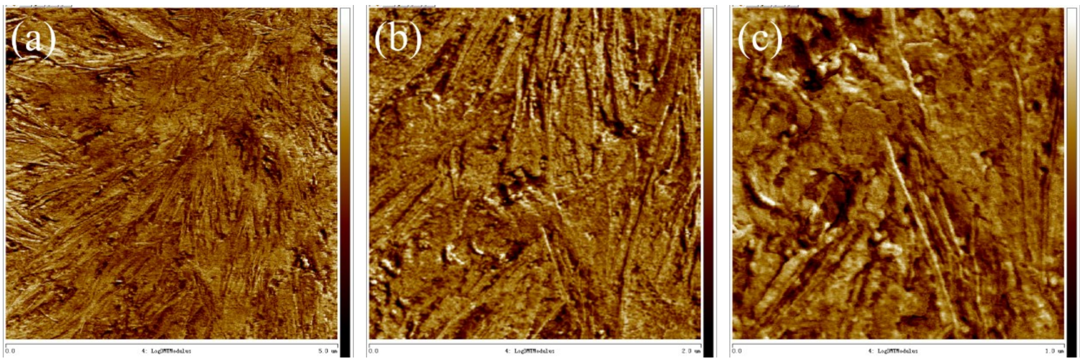

Fig. S7. AFM phase images of 30SEBS/50PEW/20LDPE. (a) 5×5μm; (b) 2×2μm; (c) 1×1μm.

AFM with PeakForce quantitative nanomechanical property mapping (QNM) mode was used to capture phase images of the ternary blends. Under PeakForce QNM mode, the formation of images is based on difference of modulus or adhesion. The brighter areas in **Fig. S7** relate to higher stiffness and thus higher crystallinity. AFM phase images also reveal the morphology of this ternary blends. Lamellae with nearly uniform distribution are clearly observed, which corresponds to the crystallization of PEW and LDPE.

2.6 POM Images of the Ternary Blends during Heating

The morphology transition of the ternary blend during heating was monitored by a POM. The melting process of the PEW and LDPE in the blends was observed from 40 ^{o}C to 110 ^{o}C at a heating rate of 2 ^{o}C min^{-1}. It proves that PEW and LDPE melted gradually when heated (**Fig. S8**). When the temperature reached about 110 ^{o}C, there was little crystalline components. POM results certified that the continuous shape recovery behavior of this ternary blends during multi-stage recovery testing was caused by sequent melting of PEW and LDPE in the elastic SEBS-network.

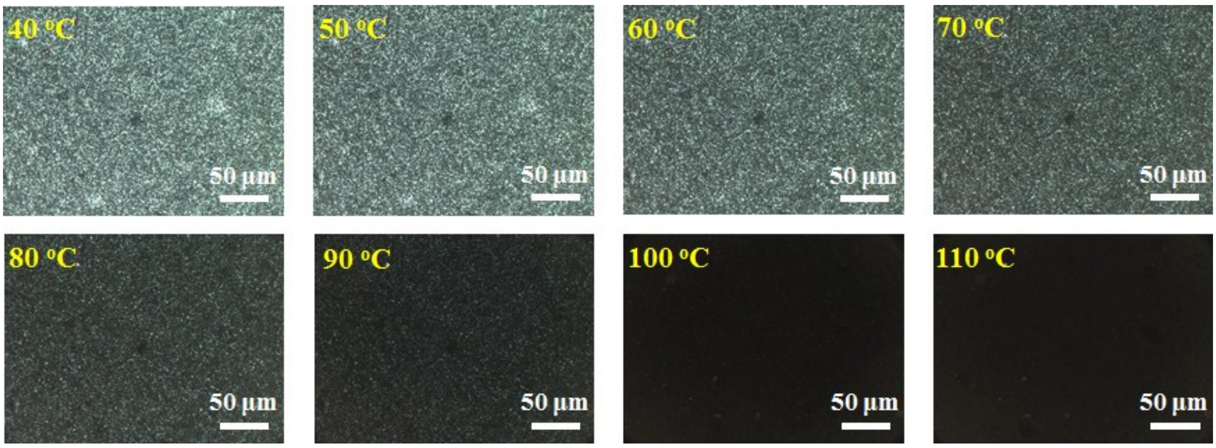

Fig. S8. POM images of the sample 30SEBS/50PEW/20LDPE during heating at 2 ^{o}C min^{-1}.

2.7 Discussion on Processability of the Blends

Two kinds of samples were tested: (i) 30 SEBS+50 PEW; (ii)30 SEBS+50 PEW+20 LDPE (mass ratio). The samples in the form of flat sheets were subjected to rheological measurements between the parallel plates of the rheometer (HAAKE MARS III, Thermofisher). The distance between two plates was about 600 μm. The deformation amplitude γ_o was set to 1%. Firstly, samples were kept at 200 ^{o}C for 5 min to eliminate heat history and then cooled to 0 ^{o}C. After waiting for 5 min, samples were reheated to the specified testing temperature. Three testing temperatures were chosen in this experiment: 150 ^{o}C, 170 ^{o}C and 190 ^{o}C. Finally, the samples were subjected to frequency-sweep testing with γ_o of 1% at 150 ^{o}C, 170 ^{o}C and 190 ^{o}C over the frequency range from 100 to 0.03 Hz. As shown in **Fig. S9**, samples with LDPE exhibit obvious frequency dependencies of G', and G'' at different testing temperatures, while samples consisting only of SEBS and PEW hardly show that. Moreover, G' and η values of ternary blends are smaller than those of binary blends during the whole testing. It demonstrates that the binary blends consisting of SBES and PEW has solid-like property for the strong phase separation of SEBS, which is difficult for extrusion process or 3D printing. The addition of LDPE convert the blends to sticky fluid and lowers the viscosity. Therefore, the ternary blends with LDPE is more suitable for extrusion and 3D printing.

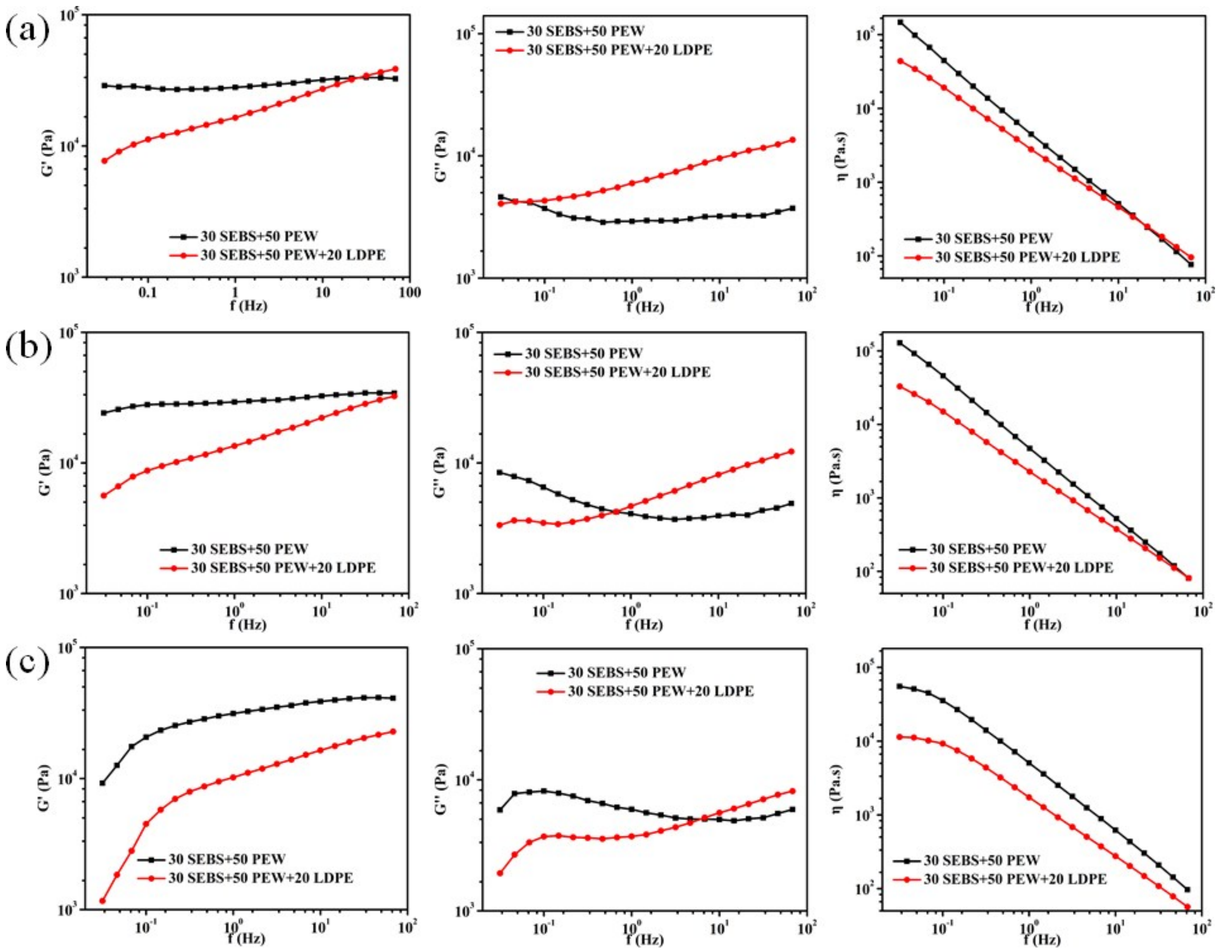

Fig. S9. Elastic modulus (G'), viscous modulus (G'') and viscosity (η) of SEBS/PEW binary blend and SEBS/PEW/LDPE ternary blend at different temperatures. (a) 150 ^{o}C. (b) 170 ^{o}C. (c) 190 ^{o}C.